Direct Detection of Effective Glass Transitions in Miscible Polymer Blends by Temperature-Modulated Differential Scanning Calorimetry

Yohei Miwa,[†] Kaori Usami,[†] Katsuhiro Yamamoto,*[,†] Masato Sakaguchi,[‡] Masahiro Sakai,[§] and Shigetaka Shimada*[,†]

Department of Materials Science & Engineering, Nagoya Institute of Technology, Gokiso-cho, Showa-ku, Nagoya 466-8555, Nagoya Keizai University, 61 Uchikubo, Inuyama, 484-8503, and Research Center for Molecular-Scale Nanoscience, Institute for Molecular Science, 38 Nishigo-Naka, Myodaiji, Okazaki 444-8585, Japan

Received September 22, 2004; Revised Manuscript Received December 17, 2004

ABSTRACT: Individual effective glass transitions of components in miscible blends of polystyrene/poly(vinyl methyl ether), poly(*o*-chlorostyrene)/poly(vinyl methyl ether), and poly(styrene-*block*-*n*-butyl acrylate)/polystyrene were detected by temperature-modulated differential scanning calorimetry. These blends apparently showed broad single glass transitions in their heat capacity (C_p) curves. This result has been widely accepted as a criterion of miscible mixing of both components. However, the derivative C_p curves of some blends showed bimodal peaks. This indicates the coexistence of two relaxations in the miscible blend. Moreover, the ratio of the two peaks was related to the compositions of the blends. The temperatures at the peaks of the derivative C_p curve were taken to be effective glass transition temperatures ($T_{g,A}$ and $T_{g,B}$) of the components in the blend. $T_{g,A}$ and $T_{g,B}$ were much different from the average glass transition temperature ($T_{g,av}$) at which the endothermic shift was half in the C_p curve. On the other hand, $T_{g,av}$ and $T_{g,A}$ of homopolymers and poly(styrene-*random*-*n*-butyl acrylate)s were almost coincident with each other. $T_{g,A}$ and $T_{g,B}$ of the blends were in excellent agreement with the effective glass transition temperatures predicted by the model, taking into account the self-concentration effect.

Introduction

The existence of a single glass transition is widely applied as a criterion of the miscible state in a polymer blend.[1−5] The cooperative conformational rearrangement in a miscible polymer blend should involve the motion of polymer segments pertaining to both components of the blend. As a result, this provides a single main dielectric or mechanical relaxation process that depends on the composition of the blend. However, distinct relaxation processes have sometimes been detected in some pairs of miscible polymer blends by experimental techniques (NMR,[1,6,7] dielectric spectroscopy,[8,9] quasielastic neutron scattering,[10] ESR,[11,12] etc.). To interpret these experimental results, concentration fluctuations (driven by the thermodynamics of the blends)[13−15] and a self-concentration effect induced by the chain connectivity[16−19] were considered mainly. Especially, the model considering the self-concentration effect proposed by Lodge and McLeish (L−M model) has widely been accepted to explain the separated average dynamics of components in miscible blends.[7,8,11,18,19] In a miscible polymer blend of polymers A and B, the chain connectivity imposes that the local environment of a segment of polymer A is (on average) necessarily richer in polymer A compared to the bulk composition (ϕ). The effective local concentration (ϕ_{eff}) sensed by a polymer segment is thus given by

$$\phi_{eff} = \phi_s + (1 - \phi_s)\phi \tag{1}$$

Here, ϕ_s is the "self-concentration" of the considered polymer segment. In the L−M model, the length scale related to the monomeric friction factor is considered to be on the same order as the Kuhn length, l_k, which is defined to be $C_\infty l$. C_∞ is the characteristic ratio, and l is the length of the average backbone bond. It is assumed that the relaxation of the Kuhn segment is influenced by the concentration of monomers within a volume $V = g l_k^3$ (g being a geometric factor).[20] ϕ_s is calculated as the volume fraction occupied by the Kuhn length's worth of monomers inside V:

$$\phi_s = C_\infty M_0 / k \rho N_{av} V \tag{2}$$

where M_0 is the molar mass of the repeat unit, N_{av} is the Avogadro number, k is the number of backbone bonds per repeat unit, and ρ is the density.

One points out that the dielectric technique etc. are able to detect microheterogeneities in the blend on a smaller length scale than those DSC can detect.[2,21] However, the DSC traces are remarkably broadened by blending.[2,11,18] Lodge and McLeish showed the simulated DSC traces based on the self-concentration, when it was assumed that the calorimetric T_g reflects the different local environments between the samples. Their simulated results described well the features of experimental DSC traces.[2,11,18] For example, the glass transitions of miscible blends are broader than those of the pure components, and the glass transition of a 25:75 blend is broader than that of a 75:25 blend of the same components (the lower T_g component listed first). This implies that the broad glass transition of a polymer blend may be caused by the superposition of effective glass transitions of the components.

Miscible polymer/solvent blends often show two distinct glass transitions in calorimetric measurements.[22−27] Recently, Savin et al. studied glass transi-

* To whom correspondence should be addressed. E-mail: yamamoto.katsuhiro@nitech.ac.jp (K.Y.); shimada.shigetaka@nitech.ac.jp (S.S.).
[†] Nagoya Institute of Technology.
[‡] Nagoya Keizai University.
[§] Institute for Molecular Science.

10.1021/ma0480401 CCC: $30.25
Published on Web 02/04/2005

tions of solvent/solvent and polymer/solvent blends by DSC.[22] The solvent/solvent mixture showed single glass transitions in any composition, and the width of the glass transition step in the DSC trace had almost no composition dependence. In contrast, the composition dependence of T_g in polymer/solvent mixtures was different at high and low polymer concentrations, and two distinct glass transitions were observed at intermediate compositions. Savin et al. interpreted these results in terms of the local length scale and local composition variations affecting T_g. In the L−M model, the lower T_g component typically has a smaller persistence length, and it leads to a larger self-concentration.[18] In polymer solutions, the solvent persistence length is negligible, implying a self-concentration approaching unity. In terms of the length scale, the solvent senses only a very local environment in the mixture and retains its own T_g. In contrast, the local composition of the polymer is affected immediately upon the addition of a small amount of the solvent. Namely, the dynamic behavior in polymer/solvent systems is analogous to that of polymer blend systems, in which the solvent is the fast component of the blend.

Temperature-modulated DSC (MDSC) is a modified version of regular DSC which uses an oscillatory heating ramp that results in increased instantaneous heating rates.[28] This modulated heating rate can increase the instrument's sensitivity and provides a stable baseline. Moreover, the slow average heating rate maintains a high resolution.

This is the first paper on the direct detection of effective glass transitions of components in miscible polymer blends by calorimetric measurements. The detection of the effective glass transitions was carried out on three systems of polystyrene/poly(vinyl methyl ether) (PS/PVME), poly(*o*-chlorostyrene)/poly(vinyl methyl ether) (P*o*ClS/PVME), and poly(styrene-*block*-*n*-butyl acrylate)/polystyrene (PS-*block*-*n*BA/PS). PS/PVME[29] and P*o*ClS/PVME[30] are well-known as pairs having a lower critical solution temperature (LCST). Effective glass transitions of components in the PS/PVME and P*o*ClS/PVME blends were detected by thermally stimulated depolarization current (TSDC) and dielectric relaxation measurement even though single glass transitions were observed by conventional DSC.[8,20] Moreover, the effective glass transition temperatures of the components were predicted well by the L−M model. PS-*block*-*n*BA shows a disordered state when its molecular weight is small. The difference in the T_g values between PS and P*n*BA is very large (∼150 K), and this is considered to be advantageous to detect effective glass transitions.

Experimental Section

Materials. Polystyrenes PS-1 and PS-2 and PVME were obtained from Tosoh and Tokyo Chemical Co., Ltd., respectively. Inhibitors in *n*BA (extrapure reagent, Tokyo Chemical), styrene (ST; extrapure reagent, Nacalai Tesque Co., Ltd.), and *o*ClS (extrapure reagent, Tokyo Chemical) were adsorbed to activate aluminum oxide (particle size 2−4 mm, Kanto Chemical Co., Inc.) and removed. Benzoyl peroxide (BPO; reagent, Nacalai Tesque), *N*,*N*,*N*′,*N*′,*N*″-pentamethyldiethylenetriamine (PMDETA; 99%, Aldrich Chemical Co., Ltd.), 1-phenylethyl bromide (1-PEBr; 95%, Tokyo Chemical), and CuBr (98%, Aldrich) were used as received. Toluene, anisole, and methanol were obtained from Nacalai Tesque (extrapure reagent) and used without further purification.

Synthesis of Samples. Polystyrene-*block*-poly(*n*-butyl acrylate)s PS-*block*-P*n*BA-1 and PS-*block*-P*n*BA-2 were synthesized by the atom transfer radical polymerization (ATRP) technique.[31] As a first component, PS was polymerized at 383 K using the CuBr/PMDETA complex and 1-PEBr as an initiator in vacuum conditions. PS was chain-extended with P*n*BA via ATRP at 353 K using CuBr and PMDETA. After the extension, the reaction mixture was purified by precipitation from toluene solution into excess methanol.

Poly(styrene-*random*-*n*-butyl acrylate) (poly(ST-*random*-*n*BA)) and P*o*ClS were polymerized in anisole using BPO as an initiator in vacuum conditions at 363 K. Compositions of PS-*block*-P*n*BA and poly(ST-*random*-*n*BA) were determined by nuclear magnetic resonance (NMR). The molecular weight (M_n) and its distribution (M_w/M_n) of all samples were determined by gel permeation chromatography (GPC) using PS standards (Tosoh). Molecular characteristics of samples used in this work are listed in Table 1.

Table 1. Molecular Characteristics of the Samples

polymer	M_n[a]	M_w/M_n[a]	ϕ_{PnBA}[b]
PS-*block*-P*n*BA-1	26.8K	1.14	0.53
PS-*block*-P*n*BA-2	34.3K	1.11	0.56
PS-1	9.1K	1.02	
PS-2	706K	1.05	
P*o*ClS	30.2K	2.30	
PVME	14.7K	3.55	
P*n*BA	12.5K	1.10	

[a] By GPC columns calibrated with PS standards. [b] By ^{1}H NMR.

Preparation of Blend Samples. All binary blends were prepared by solution casting using toluene as the solvent. Obtained films were carefully dried under vacuum, above their glass transition temperatures for 72 h, to remove the solvent completely.

Temperature-Modulated Differential Scanning Calorimetry. Thermal analysis was carried out using a 2920 modulated differential scanning calorimeter manufactured by TA Instruments operated with TA Advantage Control software version 2.6D for Windows NT. Data analysis was performed with TA Universal Analysis software version 1.0 for Windows NT. Cooling was accomplished by a TA Instruments liquid nitrogen cooling accessory (LNCA). The dry nitrogen was purged into the MDSC cell with a flow rate of 50 mL/min. The calorimeter was calibrated with an indium standard. Ca. 10 mg of sample was loaded into a nonhermetic aluminum pan. An empty pan was used as a reference. The samples were annealed in DSC instrument at ca. T_g + 30 K for 10 min, and then the temperature was lowered to ca. T_g − 70 K at 10 K/min. A modulation amplitude of 1.5 K and a period of 60 s were used at a heating rate of 3 K/min.

Gel Permeation Chromatography. GPC was carried out in the following conditions: in THF (1 mL/min) at 313 K on four polystyrene gel columns (Tosoh TSK gel GMH (bead size 7 μm) and G4000H, G2000H, and G1000H (5 μm)) that were connected to a Tosoh CCPE (Tosoh) pump and an ERC-7522 RI refractive index detector (ERMA Inc.). The columns were calibrated against standard PS (Tosoh) samples.

Nuclear Magnetic Resonance. NMR was performed on a Bruker AVANCE 200 spectrometer using deuterated chloroform at 298 K with tetramethylsilane as an internal reference.

Small-Angle X-ray Scattering (SAXS). SAXS measurement was performed at beamline BL15A in the Photon Factory (PF) of the High Energy Accelerator Research Organization (KEK) in Tsukuba, Japan, and at beamline BL40B2 in SPring 8 in Hyogo, Japan. White radiation from the source was monochromatized using a double monochromator of a Si(111) crystal to give an intense beam of $\lambda = 0.1499$ nm X-ray. The imaging plate (Rigaku R-AXIS) was used as a detector and located at distances of 1.0 m (BL40B2) and 2.3 m (BL15A) from the sample position. Collagen (chicken tendon) was used as a standard specimen to calibrate the SAXS detector. The experimental data were corrected for background scattering and sample absorption.

Static Birefringence. Static birefringence (depolarization of a transmitted light) was used to know whether the samples are miscible. Vertically polarized light from a He−Ne laser

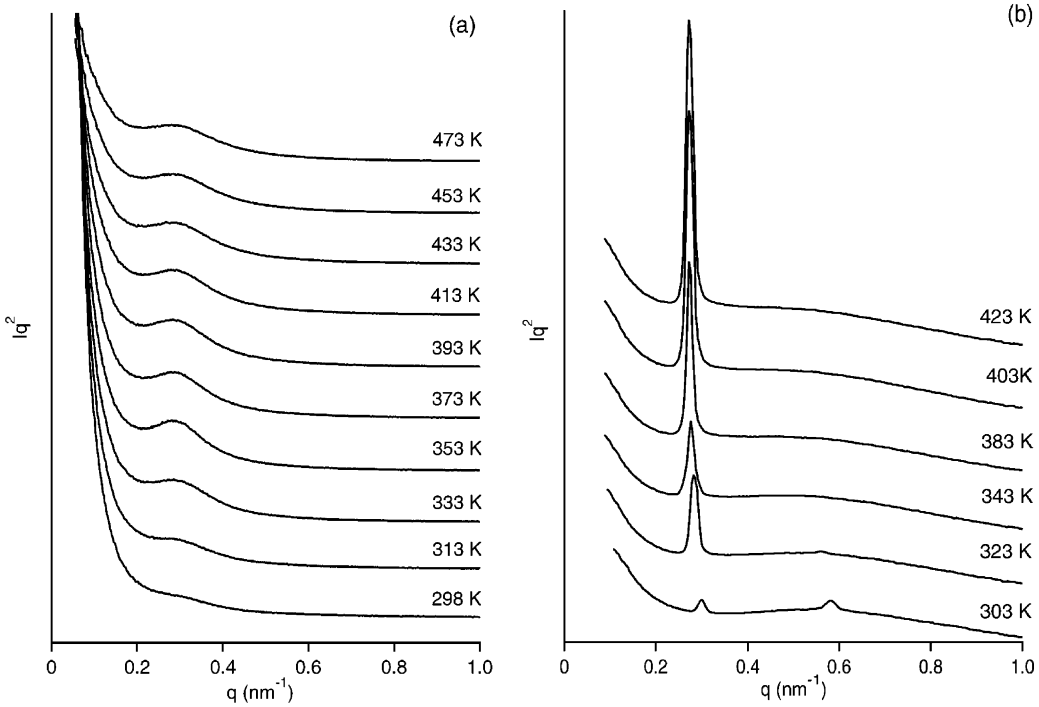

Figure 1. Temperature dependence of SAXS profiles of (a) PS-*block*-P*n*BA-1 and (b) PS-*block*-P*n*BA-2. Each profile was vertically shifted to avoid overlapping.

was directed through the sample and a horizontally polarized analyzer placed before a photodiode detector. Samples in the isotropic state (disordered state) do not depolarize the light, and no signal is recorded, whereas lamellar or hexagonal phases are birefringent. The measurements for PS-*block*-P*n*BA-1 and -2 and PS-*block*-P*n*BA-1/PS-1 blends were carried out at room temperature.

Results

Lorenz-corrected scattering profiles ($I\mathbf{q}^2$) of PS-*block*-P*n*BA-1 and PS-*block*-P*n*BA-2 measured in the temperature range of 298−473 K are shown in parts a and b, respectively, of Figure 1. Here, **q** is a scattering vector ($\mathbf{q} = (4\pi/\lambda)\sin(\theta/2)$; θ is the scattering angle). A broad peak and weak intensity were observed for PS-*block*-P*n*BA-1 (Figure 1a). The weak scattering intensity was caused by the small electron density difference between the (0.565 mol/cm^3) and P*n*BA (0.590 mol/cm^3).[32] In addition, PS and the P*n*BA have similar solubility parameters (8.7 and 8.8 (cal/cm^3)$^{0.5}$, respectively), and this means a weak segregation pair.[33] The SAXS profiles seem to suggest a disordered state of the sample. Additionally, obvious distinct glass transitions of each component were not observed in the MDSC curve (see Figure 4b). Therefore, we consider that PS-*block*-P*n*BA-1 is in a disordered state. On the other hand, PS-*block*-P*n*BA-2 showed sharp and multiple scattering peaks from the microphase separation (Figure 1b) and clear distinct T_g values of each component in the MDSC trace (see Figure 4b). A lamellar morphology is expected from the integrate reflections and the even composition of PS-*block*-P*n*BA-2.

Furthermore, the miscibility of PS-*block*-P*n*BA-1 and PS-*block*-P*n*BA-1/PS-1 blends was examined by a static birefringence measurement. In contrast with PS-*block*-P*n*BA-2, which showed birefringence, PS-*block*-P*n*BA-1 and PS-*block*-P*n*BA-1/PS-1 blends showed no birefringence. This result also supports the miscible state in PS-*block*-P*n*BA-1 and PS-*block*-P*n*BA-1/PS-1 blends.

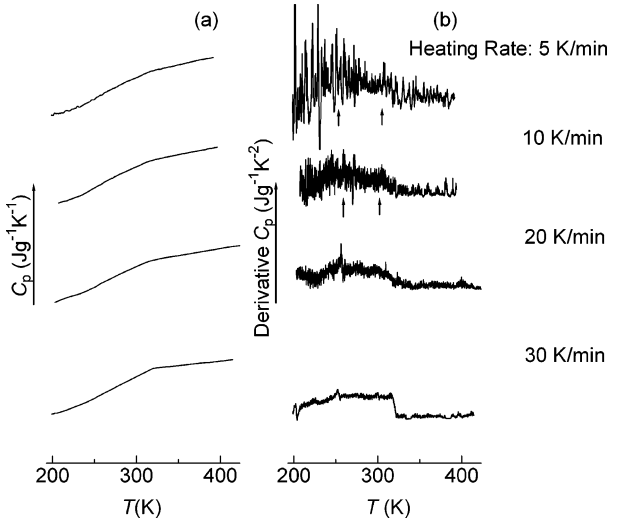

Figure 2. (a) C_p curves of PS-*block*-P*n*BA-1 measured by conventional DSC at heating rates of 5, 10, 20, and 30 K/min. (b) Derivative C_p curves. $T_{g,A}$ and $T_{g,B}$ are assigned with arrows.

Heat capacity (C_p) and derivative C_p curves of PS-*block*-P*n*BA-1 measured by conventional DSC at heating rates of 5, 10, 20, and 30 K/min are shown in parts a and b, respectively, of Figure 2. The C_p and the derivative C_p curves of poly(ST-*random*-*n*BA), PS-*block*-P*n*BA-1/PS-1, P*o*ClS/PVME, and PS-2/PVME measured by MDSC are shown in Figures 3−6, respectively. The C_p and derivative C_p curves of PS-*block*-P*n*BA-2 are shown in Figure 4. The blends apparently showed single glass transitions in their C_p curves. Therefore, it is considered that the components are compatibly mixing in the blends.[20,29,30] However, some blends showed bimodal peaks in the derivative C_p curves in contrast with single peaks of homopolymers and random copolymers. The bimodal peaks in the derivative C_p curves indicate that two relaxations coexist in the miscible blends.

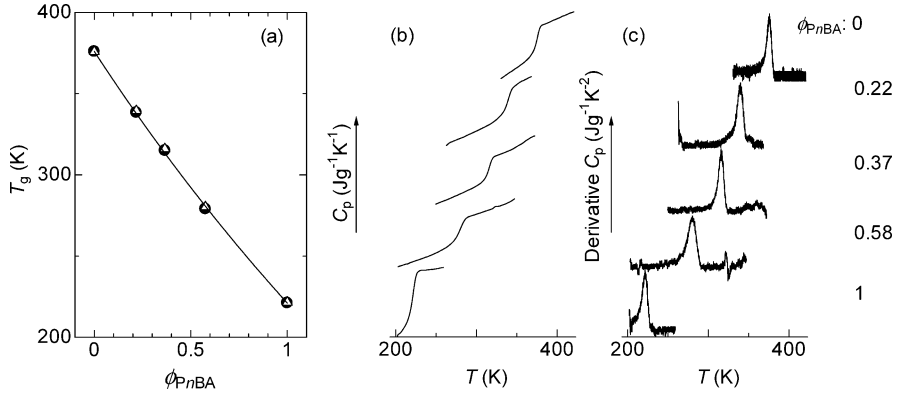

Figure 3. (a) $T_{g,av}$ (circles) and $T_{g,A}$ (triangles) of poly(ST-*random*-*n*BA) against ϕ_{PnBA}. The solid curve is determined by the Gordon−Taylor equation with $K = 0.85$. (b) C_p curves. (c) Derivative C_p curves.

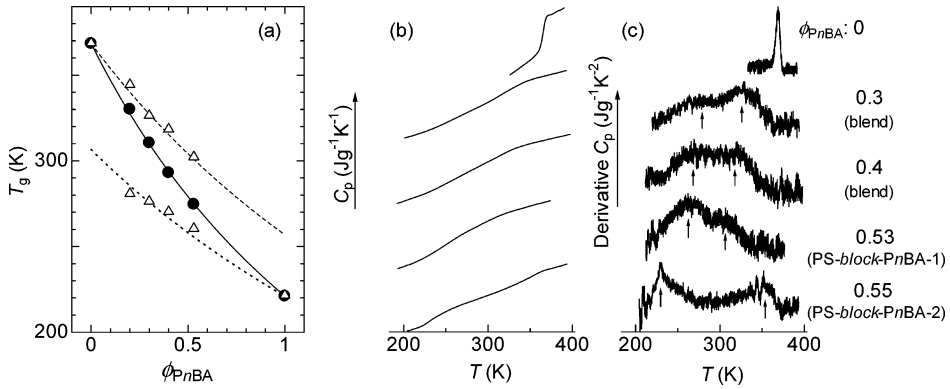

Figure 4. (a) $T_{g,av}$ (circles) and $T_{g,A}$ and $T_{g,B}$ (triangles) of PS-*block*-P*n*BA-1/PS-1 blends against ϕ_{PnBA}. Dashed and dotted curves are $T_{g,eff}$ values for the PS and P*n*BA components, respectively, calculated by the L−M model. The solid curve is determined by the Gordon−Taylor equation with $K = 0.65$. (b) C_p curves of PS-*block*-P*n*BA-1, PS-*block*-P*n*BA-1/PS-1 blends, and PS-*block*-P*n*BA-2. (c) Derivative C_p curves. $T_{g,A}$ and $T_{g,B}$ are assigned with arrows.

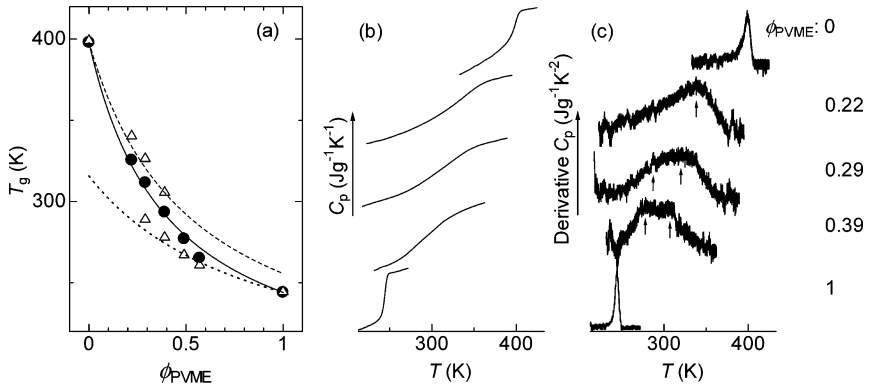

Figure 5. (a) $T_{g,av}$ (circles) and $T_{g,A}$ and $T_{g,B}$ (triangles) of P*o*ClS/PVME blends against ϕ_{PVME}. Dashed and dotted curves are T_{geff} values for the P*o*ClS and PVME components, respectively, calculated by the L−M model. The solid curve is determined by the Gordon−Taylor equation with $K = 0.3$. (b) C_p curves. (c) Derivative C_p curves. $T_{g,A}$ and $T_{g,B}$ are assigned with arrows.

In this paper, T_g was defined by two methods. In the first method the midpoint of the glass transition step in the C_p curve, i.e., the temperature corresponding to half of the endothermic shift, was taken as $T_{g,ave}$. In the second one the temperature at the peak of the derivative C_p curve was taken. Here, some blends showed two peaks in their derivative C_p curves. Therefore, the temperatures at the lower and upper peaks were defined as $T_{g,A}$ and $T_{g,B}$, respectively. These values of poly(ST-*random*-*n*BA) and PS-*block*-P*n*BA-1/PS-1 were plotted against the weight fraction of P*n*BA (ϕ_{PnBA}) in Figures 3a and 4a, respectively. Similarly, $T_{g,av}$, $T_{g,A}$, and $T_{g,B}$ of P*o*ClS/PVME and PS-2/PVME were plotted against the weight fraction of PVME (ϕ_{PVME}) in Figures 5a and 6a, respectively. $T_{g,av}$ was fitted by the Gordon−Taylor equation.[34] The Gordon−Taylor equation is given by

$$T_g(\phi_X) = (T_{g,X}\phi_X + KT_{g,Y}(1 - \phi_X))/(\phi_X + K(1 - \phi_X)) \quad (3)$$

where ϕ_X is the bulk weight fraction of the lower T_g component X. $T_{g,X}$ and $T_{g,Y}$ are the T_g values of pure polymers X and Y, respectively. K is a fitting parameter.

The broadness of the glass transitions (ΔT_g) $T_{g,i}$, and $T_{g,e}$ of poly(ST-*random*-*n*BA) and PS-*block*-P*n*BA-1/PS-1 are compared in Figure 7. ΔT_g, $T_{g,i}$, and $T_{g,e}$ are defined as shown in the figure.

$T_{g,av}$, $T_{g,A}$, $T_{g,B}$, $T_{g,i}$, and $T_{g,e}$ of poly(ST-*random*-*n*BA) and PS-*block*-P*n*BA-1/PS-1 are listed in Table 2. Simi-

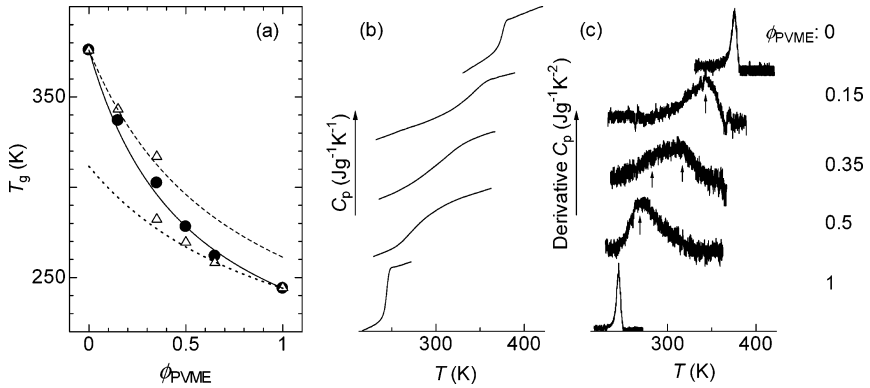

Figure 6. (a) $T_{g,av}$ (circles) and $T_{g,A}$ and $T_{g,B}$ (triangles) of PS-2/PVME blends against ϕ_{PVME}. Dashed and dotted curves are $T_{g,eff}$ values for the PS and PVME components, respectively, calculated by the L−M model. The solid curve is determined by the Gordon−Taylor equation with $K = 0.35$. (b) C_p curves. (c) Derivative C_p curves. $T_{g,A}$ and $T_{g,B}$ are assigned with arrows.

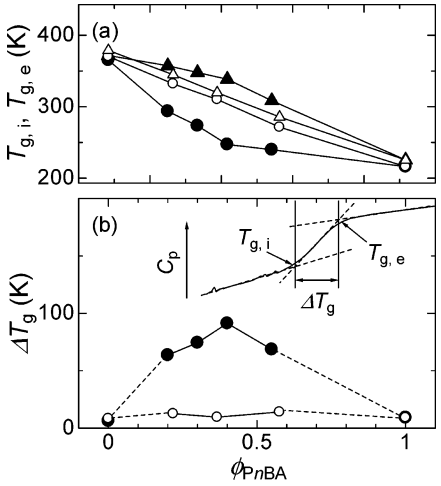

Figure 7. (a) $T_{g,i}$ (circles) and $T_{g,e}$ (triangles) against ϕ_{PnBA}. These values of poly(ST-*random*-*n*BA) and the PS-*block*-P*n*BA-1/PS-1 blend are presented as open and solid symbols, respectively. (b) ΔT_g of poly(ST-*random*-*n*BA) (open) and the PS-*block*-P*n*BA-1/PS-1 blend (solid) against ϕ_{PnBA}. The definitions of $T_{g,i}$, $T_{g,e}$, and ΔT_g are shown in the figure.

Table 2. T_g Values of PS-*block*-P*n*BA-1/PS-1 Blends and Poly(ST-*random*-*n*BA)

sample	ϕ_{PnBA}	$T_{g,av}$ (K)	$T_{g,A}$ (K)	$T_{g,B}$ (K)	$T_{g,i}$ (K)	$T_{g,e}$ (K)
PS-*block*-P*n*BA-1	0.53	275	261	302	240	308
PS-*block*-P*n*BA-1/PS-1	0.2	330	281	344	294	357
PS-*block*-P*n*BA-1/PS-1	0.3	310	276	326	273	348
PS-*block*-P*n*BA-1/PS-1	0.4	293	270	319	247	338
poly(ST-*random*-*n*BA)	0.22	338	339		332	345
poly(ST-*random*-*n*BA)	0.37	315	316		310	320
poly(ST-*random*-*n*BA)	0.58	279	280		271	286
PS-1	0	368	369		365	372
PS-2	0	376	376		370	379
P*n*BA	1	221	222		216	225

larly, those of P*o*ClS/PVME and PS-2/PVME are shown in Table 3.

Discussion

ΔT_g of PS-*block*-P*n*BA-1/PS-1 was much larger than those of PS, P*n*BA, and poly(ST-*random*-*n*BA) (Figure 7). The repeat sequence of the ST and *n*BA units of PS-*block*-P*n*BA and PS is considered to cause the broad distribution of τ_c of the α relaxation process in the blends. This behavior is generally observed in miscible polymer blends.[11,17,18,35] Lodge and McLeish pointed out that this broad ΔT_g of miscible blends was caused by the self-concentration of components induced by chain connectivity.[18] On the other hand, ΔT_g of poly(ST-*random*-*n*BA) was almost the same with those of the PS and P*n*BA homopolymers. This indicates that local heterogeneity in the random copolymer is smaller than that in the blend because the random sequence of the ST and *n*BA units in the poly(ST-*random*-*n*BA) chain gives an extremely small self-concentration. The same result was previously reported in the system of poly(cyclohexyl methacrylate-*random*-cyclohexyl acrylate).[11]

Table 3. T_g Values of P*o*ClS/PVME and PS-2/PVME Blends

sample	ϕ_{PVME}	$T_{g,av}$ (K)	$T_{g,A}$ (K)	$T_{g,B}$ (K)	$T_{g,i}$ (K)	$T_{g,e}$ (K)
P*o*ClS/PVME	0.22	326		340	298	359
P*o*ClS/PVME	0.29	312	289	326	276	347
P*o*ClS/PVME	0.39	293	278	306	264	323
P*o*ClS/PVME	0.49	277	267		256	297
P*o*ClS/PVME	0.57	265	261		251	281
PS-2/PVME	0.15	337		343	321	357
PS-2/PVME	0.35	302	282	316	273	332
PS-2/PVME	0.5	278	270		256	300
PS-2/PVME	0.65	262	258		250	274
P*o*ClS	0	398	399		391	404
PS-2	0	376	376		370	379
PVME	1	244	244		241	247

$T_{g,av}$ and $T_{g,A}$ of the homopolymers and poly(ST-*random*-*n*BA) were almost coincident with each other (Figure 3a and Table 2). However, $T_{g,A}$ and $T_{g,B}$ of the blends were much different from their $T_{g,av}$ values (Figures 4a, 5a, and 6a). In addition, some blends showed bimodal peaks in the derivative C_p curves (Figures 4c, 5c, and 6c). The bimodal peaks in the derivative C_p curve indicate the coexistence of two relaxations in the miscible blend. The ratio of the peaks was related to the composition of the blend; e.g., the height of the right peak in the derivative C_p curve of PS-*block*-P*n*BA-1/PS-1 increased with an increase in the PS component. This result supported that the bimodal peaks were caused by the individual effective glass transitions of the components in the blend. The bimodal peaks of PS-*block*-P*n*BA-1/PS-1 were the most obvious in the samples studied in this work because the difference in the T_g values between PS and P*n*BA was the largest. These results demonstrated that the broad glass transitions in DSC curves of miscible polymer blends were caused by the superposition of individual effective glass transitions of components as Lodge and McLeish pointed out.[18]

Moreover, it was interesting that the effective glass transitions of PS-*block*-P*n*BA-1 were detected by the conventional DSC measurement (Figure 2). The deriva-

tive C_p curves measured at heating rates of 5 and 10 K/min were somewhat noisy because of the low sensitivity due to the slow scan, but bimodal peaks were observed. On the other hand, it was hard to find the bimodal peaks in the derivative C_p curves measured at 20 and 30 K/min. The sensitivity of DSC increased with an increase in the heating rate. However, it seemed that the temperature resolution decreased with an increase in the heating rate. These results suggest that conventional DSC is also able to detect effective glass transitions of components in miscible polymer blends. Namely, the resolution of conventional DSC might be as good as that of MDSC when the heating rate is slow. However, it is obvious that MDSC is advantageous for the detection of effective glass transitions in miscible blends. The reason MDSC is superior to conventional DSC to detect effective glass transitions is that the stable baseline, the high sensitivity, and the high resolution are compatible. Measurement conditions of MDSC (modulation amplitude, a modulation period, and an average heating rate) did not affect the results although $T_{g,A}$ and $T_{g,B}$ were somewhat shifted depending on the difference of instantaneous heating rates. The most suitable conditions were a modulation amplitude of 1.5 K, a modulation period of 60 s, and a heating rate of 3 K/min (see the Supporting Information). Effects of the measurement conditions are shown in the Supporting Information.

Leroy et al. detected effective glass transitions of components in P*o*ClS/PVME and PS/PVME by TSDC.[20] They showed that the experimental effective glass transition temperatures agreed well with the ones predicted by the L−M model considering the self-concentration effect. Moreover, Leroy et al. proposed a model which took into account both effects, the self-concentration and the concentration fluctuation, and the model agreed well with their experimental results.[8] Their model was based on the idea that the average mobility of each component in the blends is affected by an effective concentration induced by the self-concentration effect, and the distribution of the mobility of each component is mainly due to the concentration fluctuation.

Recently, Savin et al. observed two distinct glass transitions in polymer/solvent mixtures by DSC.[22] They interpreted this result in terms of the local composition variations caused by the self-concentration effect. In fact, two distinct glass transitions and an increase in the width of the glass transition region were not observed for solvent/solvent mixtures. In a solvent/solvent mixture, no self-concentration effect is expected because there is no chain connectivity of the solvent molecules.

$T_{g,A}$ and $T_{g,B}$ of the blends were compared to the effective T_g ($T_{g,eff}$) calculated by the L−M model (Figures 4a, 5a, and 6a).[18] In the L−M model, $T_{g,eff}$ is assumed as follows:

$$T_{g,eff}(\phi) = T_g(\phi)|_{\phi=\phi_{eff}} \quad (4)$$

where $T_g(\phi)$ corresponds to T_g of a blend of average concentration ϕ. The evolution of $T_{g,eff}$ was calculated by combining eqs 1, 3, and 4. For example, $T_{g,eff}$ of component A is given by

$$T_{g,eff,X}(\phi_X) = (T_{g,X}\phi_{eff,X} + KT_{g,Y}(1 - \phi_{eff,X}))/(\phi_{eff,X} + K(1 - \phi_{eff,X})) \quad (5)$$

where $\phi_{eff,X}$ is the effective concentration of the X component, calculated using eq 1. The self-concentrations, ϕ_s, of PS, P*o*ClS, and PVME were reported to be 0.27, 0.22, and 0.25, respectively.[18,20] ϕ_s of P*n*BA is calculated to be ca. 0.42.[36] Recently, Lutz et al. investigated the dynamics of isolated polyisoprene chains in host matrixes of polybutadiene, poly(vinylethylene), and PS by NMR.[37] They concluded that ϕ_s in the L−M model was affected by matrixes, and small adjustment of the length scale by the geometric factor g used to calculate the volume V was effective to fit the experimental results. In the case of the PS-*block*-P*n*BA-1/PS-1 blends, the g values of PS and P*n*BA were found to be ca. 0.8 and 1.3, respectively.

Remarkably good agreements of $T_{g,A}$ and $T_{g,B}$ with calculated $T_{g,eff}$ curves were observed in the PS-*block*-P*n*BA-1/PS-1, P*o*ClS/PVME, and PS-2/PVME blends (Figures 4a, 5a, and 6a). These results imply that the effective glass transitions detected by MDSC are caused by the self-concentration of components induced by chain connectivity.

The effective mobility of components in miscible blends has often been detected by NMR,[1,6,7] dielectric spectroscopy,[8,9] quasielastic neutron scattering,[10] ESR,[11,12] etc. The single glass transition in the DSC measurement has been widely applied as an effective criterion of miscible mixing of both components. However, the results shown in this work obviously indicate that DSC is able to detect effective glass transitions of components in miscible polymer blends. Moreover, the superposition of effective glass transitions of components is the cause of a broad glass transition in a DSC trace of a miscible polymer blend.

Conclusion

Individual effective glass transitions of components in miscible blends of PS/PVME, P*o*ClS/PVME, and PS-*block*-P*n*BA/PS were detected as double peaks in the derivative C_p curves. MDSC was superior to conventional DSC for the detection of the effective glass transitions in miscible blends although conventional DSC was also able to detect the effective glass transitions. The effective glass transitions were the most obvious in PS-*block*-*n*BA/PS because the difference in the T_g values of PS and P*n*BA was the largest (∼150 K) in this study. These results demonstrated that the broadness of a glass transition in a DSC curve of a miscible blend was caused by the superposition of individual effective glass transitions of the components. $T_{g,A}$ and $T_{g,B}$ of the blends were in good agreement with $T_{g,eff}$ calculated by the L−M model. This result implies that the effective glass transitions detected by MDSC are caused by the self-concentration of components induced by chain connectivity. An apparent single glass transition in a DSC trace is a useful criterion of a miscible state in a polymer blend. However, the superposition of effective glass transitions of components is the cause of the apparent single glass transition in a DSC trace of a miscible polymer blend, and DSC is also able to detect the effective glass transitions of components in miscible polymer blends.

Acknowledgment. Thanks are due to the Research Center for Molecular-Scale Nanoscience, the Institute for Molecular Science, for assistance in obtaining the DSC data. This research was supported by the Ministry of Education, Science, Sports and Culture, Grant-in-Aid

for Young Scientists (B), 16750185, 2004. The SAXS measurement was performed under approval of the Photon Factory Program Advisory Committee (Proposal No. 2003G275) and SPring8 Program Advisory Committee(Proposal No. 2004A0227-NL2b-np).

Supporting Information Available: C_p and derivative C_p curves of PS-*block*-PnBA-1. This material is available free of charge via the Internet at http://pubs.acs.org.

References and Notes

(1) Lau, C.; Mi, Y. *J. Polym. Sci., Part B: Polym. Phys.* **2001**, *39*, 2390.
(2) Pellerin, C.; Pelletier, I.; Pézolet, M.; Prud'homme, R. E. *Macromolecules* **2003**, *36*, 153.
(3) Aubin, M.; Prud'homme, R. E. *Macromolecules* **1988**, *21*, 2945.
(4) Lau, S.; Pathak, J.; Wunderlich, B. *Macromolecules* **1982**, *15*, 1278.
(5) Cowie, J. M. G.; Harris, S.; Ribelles, J. L.; Meseguer, J. M.; Romero, F.; Torregrosa, C. *Macromolecules* **1999**, *32*, 4430.
(6) Min, B.; Qiu, X.; Ediger, M. D.; Pitsikalis, M.; Hadjichristidis, N. *Macromolecules* **2001**, *34*, 4466.
(7) Haley, C. J.; Lodge, P. T.; He, Y.; Ediger, M. D.; von Meerwall, E. D.; Mijovic, J. *Macromolecules* **2003**, *36*, 6142.
(8) Leroy, E.; Alegria, A.; Colmenero, J. *Macromolecules* **2003**, *36*, 7280.
(9) Urakawa, O.; Fuse, Y.; Hori, H.; Tran-Cong, Q.; Yano, O. *Polymer* **2001**, *42*, 765.
(10) Hoffmann, S.; Willner, L.; Richter, D.; Arbe, A.; Colmenero, J.; Farago, B. *Phys. Rev. Lett.* **2000**, *85*, 772.
(11) Miwa, Y.; Sugino, Y.; Yamamoto, K.; Tanabe, T.; Sakaguchi, M.; Sakai, M.; Shimada, S. *Macromolecules* **2004**, *37*, 6061.
(12) Miwa, Y.; Tanabe, T.; Yamamoto, K.; Sugino, Y.; Sakaguchi, M.; Sakai, M.; Shimada, S. *Macromolecules* **2004**, *37*, 8612.
(13) Kumar, S. K.; Colby, R. H.; Anastasiadis, S. H.; Fytas, G. *J. Chem. Phys.* **1996**, *105*, 377.
(14) Zetsche, A.; Fischer, E. W. *Acta Polym.* **1994**, *45*, 168.
(15) Kamath, S.; Colby, R. H.; Kumar, S. K.; Karatasos, K.; Floudas, G.; Fytas, G.; Roovers, J. E. L. *J. Chem. Phys.* **1999**, *111*, 6121.
(16) Chung, G.-C.; Kornfield, J. A.; Smith, S. D. *Macromolecules* **1994**, *27*, 964.
(17) Chung, G.-C.; Kornfield, J. A.; Smith, S. D. *Macromolecules* **1994**, *27*, 5729.
(18) Lodge, T. P.; McLeish, T. C. B. *Macromolecules* **2000**, *33*, 5278.
(19) He, Y.; Ediger, M. D. *J. Chem. Phys.* **2003**, *19*, 9956.
(20) Leroy, E.; Alegria, A.; Colmenero, J. *Macromolecules* **2002**, *35*, 5587.
(21) Miller, J. B.; McGrath, K. J.; Roland, C. M.; Trask, C. A.; Garroway, A. N. *Macromolecules* **1990**, *23*, 4543.
(22) Savin, D. A.; Larson, A. M.; Lodge, T. P. *J. Polym. Sci., Part B: Polym. Phys.* **2004**, *42*, 1155.
(23) Scandola, M.; Ceccorulli, G.; Pizzoli, M. *Polymer* **1987**, *28*, 2081.
(24) Riande, E.; Markovitz, H.; Plazek, D. J.; Raghupathi, N. *J. Polym. Sci., Polym. Symp.* **1975**, *50*, 405.
(25) Ceccorulli, G.; Pizzoli, M.; Scandola, M. *Polymer* **1987**, *28*, 2077.
(26) Feldstein, M. M.; Roos, A.; Chevallier, C.; Creton, C.; Dormidontova, E. E. *Polymer* **2003**, *44*, 1819.
(27) Taniguchi, N.; Urakawa, O.; Adachi, K. *Macromolecules* **2004**, *37*, 7832.
(28) Sauerbrunn, S. R.; Crowe, B. S.; Reading, M. *Polym. Mater. Sci. Eng.* **1993**, *68*, 269.
(29) Cendoya, I. M.; Alegria, A.; Colmenero, J.; Grimm, H.; Richter, D.; Frick, B. *Macromolecules* **1999**, *32*, 4065.
(30) Tran-Cong, Q.; Nakano, H.; Okinaka, J.; Kawakubo, R. *Polymer* **1994**, *35*, 1242.
(31) Cassebras, M.; Pascual, S.; Polton, A.; Tardi, M.; Vairon, J.-P. *Macromol. Rapid Commun.* **1999**, *20*, 261.
(32) The electron density was calculated from the polymer mass density at 298 K (*Polymer Handbook*, 3rd ed.; John Wiley & Sons: New York, 1989).
(33) *Polymer Handbook*, 3rd ed.; John Wiely & Sons: New York, 1989.
(34) Gordon, M.; Taylor, S. J. *J. Appl. Chem.* **1952**, *2*, 4.
(35) Kim, E.; Kramer, E. J.; Wu, W. C.; Garrett, P. D. *Polymer* **1994**, *35*, 5706.
(36) ϕ_s of P*n*BA was calculated using $M_0 = 128$ g/mol, $\rho = 1.08$ g/cm^3 (*Polymer Handbook*, 3rd ed.; John Wiley & Sons: New York, 1989), and $k = 2$. C_∞ was calculated from the radius of gyration at the θ state and the degree of polymerization (Mathakiya, I.; Rakshit, A. K.; Rao, P. V. C. *Int. J. Polym. Anal. Charact.* **2003**, *8*, 339). C_∞ and l_k were 8.1 and 12.4 Å, respectively.
(37) Lutz, T. R.; He, Y.; Ediger, M. D.; Pitsikalis, M.; Hadjichristidis, N. *Macromolecules* **2004**, *37*, 6440.

MA0480401